Beyond spin-magnetism of magnetic nanowires in porous silicon

2008 J. Phys.: Condens. Matter 20 454221

(http://iopscience.iop.org/0953-8984/20/45/454221)

J. Phys.: Condens. Matter **20** (2008) 454221 (5pp) doi:10.1088/0953-8984/20/45/454221

Beyond spin-magnetism of magnetic nanowires in porous silicon

K Rumpf, P Granitzer and H Krenn

Institute of Physics, Karl Franzens Universität Graz, Universitätsplatz 5, A-8010 Graz, Austria

E-mail: heinz.krenn@uni-graz.at

Received 18 June 2008, in final form 30 September 2008
Published 23 October 2008
Online at stacks.iop.org/JPhysCM/20/454221

Abstract

A ferromagnet–semiconductor (Si–Ni-) nanowire composite, electrochemically prepared in an n-doped (001) silicon wafer, is studied using SQUID magnetometry at magnetic fields up to 7 T parallel and perpendicular to the Ni-wires (diameter 50 nm, length 1 μm, 4×10^8 wires mm^{-2}). Apart from the conventional spin-magnetism of Ni which is saturated at low field, an additional giant paramagnetism is observed at fields >1 T, which is nearly temperature independent, shows strict linear field dependence, strong anisotropy and a lack of saturation. Taking the difference of the orthogonal magnetizations this unconventional paramagnetism becomes obvious. It is based on mesoscopic currents driven by the symmetry breaking at the wire–silicon interface due to the Rashba field (spin-galvanic effect). Spin-polarized carriers from the Ni-wires are captured in low angular momentum quantum states ($\ell = 1, 2, \ldots$). An attempt has been made to estimate the observed giant magnetic moment under simplifying assumptions.

1. Introduction

One-dimensional nanostructures have attracted great attention for basic research and applications. An inexpensive route to their structural design is the deposition of metallic nanowires in a templated substrate using electrochemical deposition in alumina or polymer membranes [1–3]. Magnetic nanowires are of special interest due to the interplay of spin-, orbit- and charge-related physical phenomena [4]. The magnetization dynamics has been investigated since the late 1950s [5]. The various modes of magnetization reversal and hysteresis in reduced-dimensional systems such as nanowires is still an interesting research field with a strong impact on applications, e.g. magnetic data recording.

This work goes beyond the micromagnetics of nanowires. It includes the interaction with the matrix in which the wires are embedded. Mostly the matrix (polymer, insulator) is not taken into account as mediating any interaction between magnetic nanowires except for acting as a quantum barrier in magneto-tunneling junctions. Magnetic nanowires embedded in a *semiconducting* matrix provide additional spin and charge degrees of freedom. The doping or controllable depletion of carriers in the semiconductor *between* the wires provides an additional control for novel magneto-optic and spintronic transport properties such as optical spin-pumping, the spin-Hall effect [6, 7] and spin-galvanic effects [8]. On gold surfaces and gold particles, which are capped by organic molecules, a novel kind of 'giant orbital' magnetism has been discovered with unexpected properties. Enhanced magnetic moment, non-saturation and strong geometrically induced magnetic anisotropy [9] have been observed. For an explanation of the giant orbital magnetism two fundamental mechanisms have been proposed: on the one hand (i) persistent orbital currents are induced by spin–orbit interaction due to the symmetry-breaking interface potential. Such persistent currents generate a spin-dependent topological flux passing through the cross-section of the orbit, e.g. of a carbon nanotube [10]. On the other hand (ii) triplet pairing of injected carriers and Bose-condensation into an odd-integer orbital quantum state [11] provides a non-vanishing angular momentum and accordingly giant paramagnetism.

Since bulk silicon has inversion symmetry and the spin–orbit interaction is negligible in comparison with III–V-semiconductors or capped gold nanoparticles, and in addition the spin-relaxation—if excess spins are pumped into silicon—is less effective, this opens up the capability to manipulate the excess spins in reasonable timescales to achieve a sizable spin-accumulation.

We shall present a quantitative estimate of the giant orbital magnetism in Ni-filled porous silicon nanochannels. In the experiment a clear distinction will be reached between spin- and orbital-magnetism.

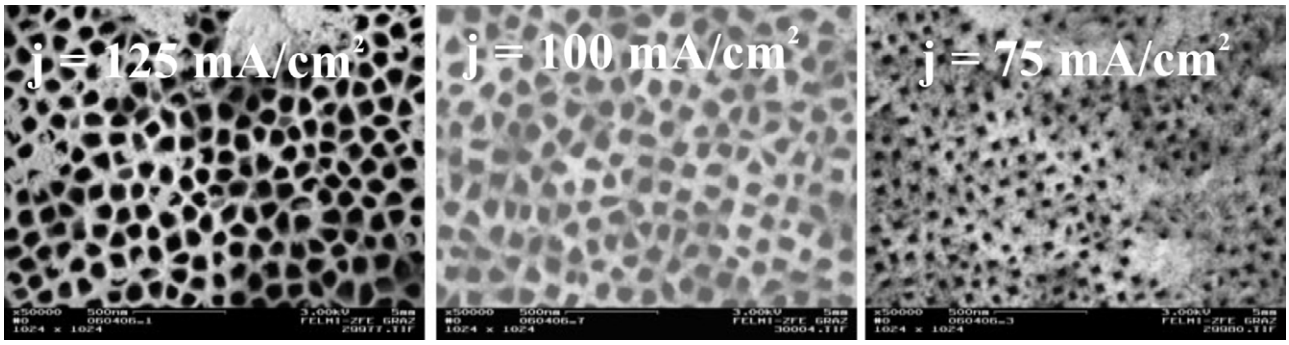

Figure 1. Top-view scanning electron micrographs of PS-samples prepared with different current densities. The pore-diameter is only moderately influenced, but the interconnecting Si-spacers and the regularity of pores is predominantly influenced by the current density.

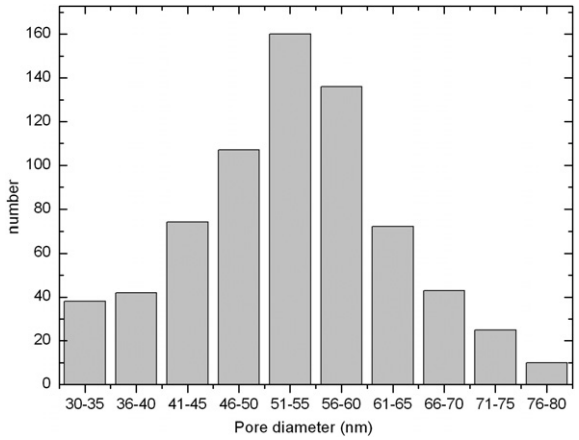

Figure 2. Histogram of a typical pore-size distribution.

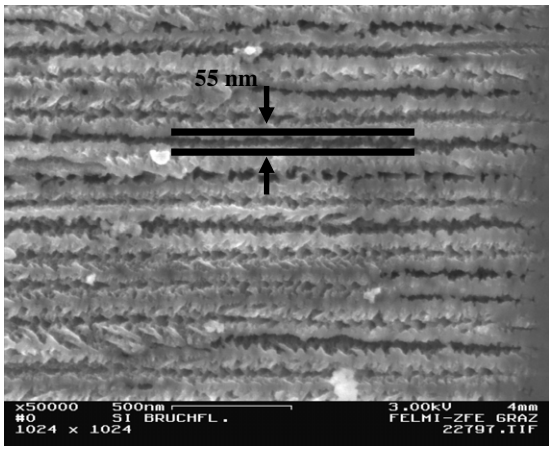

Figure 3. Cross-sectional SEM-image: the average pore-diameter is 55 nm. The side-pores occurring exhibit a length scale smaller than the pore-distance.

2. Experiments: self-assembled Ni-nanowires in a porous silicon matrix

Porous silicon (PS) can be fabricated using various electrolyte compositions; the most common are aqueous hydrofluoric acid solution, organic electrolytes and solutions containing oxidizing agents [12]. Anodization of silicon in an aqueous HF-solution generally leads to a nanostructured, branched network-like structure with dimensions between 2 and 4 nm. This so-called microporous silicon which shows light emitting properties in the visible has been investigated intensely in the 1990s [13]. In applying modified etching parameters or/and using wafers with distinct doping concentrations it is possible to achieve different morphologies of the porous structure. The dimensions can be extended to meso (5–50 nm) and macropores (>50 nm up to a few ten microns).

The structures fabricated in this work exhibit pore-diameters between 30 and 100 nm and can be attributed to the transition region between meso and macroporous silicon depending on the process parameters. Both types of porous structures, meso and macropores, exhibit a growth mechanism which depends on the crystallographic orientation of the substrate [14]. In contrast, the formation of microporous silicon is independent of the crystallographic orientation of the substrate. The meso/macroporous silicon consists of highly oriented pores, which grow perpendicular to the sample surface, exhibiting a length up to 50 μm. The pores are arranged in a quasi-four-fold coordination, which is demonstrated by FT-images [15] gained from top-view scanning electron micrographs (figure 1). A typical pore-size distribution can be seen in figure 2. The scatter of the nominal pore-diameter 55 nm is usually ± 8 nm indicating a quite high homogeneity if one considers that the samples are fabricated by self-organization without any pre-structuring. With decreasing pore-diameter the square-like arrangement becomes disordered. The growth of dendrites could not be suppressed completely in the investigated morphologies, which strongly depend on the pore-diameter and on the pore-distance, respectively. If the pore-distance increases with decreasing current density, side-pores grow in the ⟨111⟩-direction but the growth-rate is much smaller than in the ⟨100⟩-direction [14]. The samples show pores significantly separated from each other (figure 3).

In a second electrochemical step metal is precipitated within the 'bare' pores of the PS-layer under cathodic electroplating. The metal deposition is carried out using a metal-salt solution as the electrolyte. To obtain Ni-nanostructures either a $NiCl_2$ or $NiSO_4$ electrolyte is used.

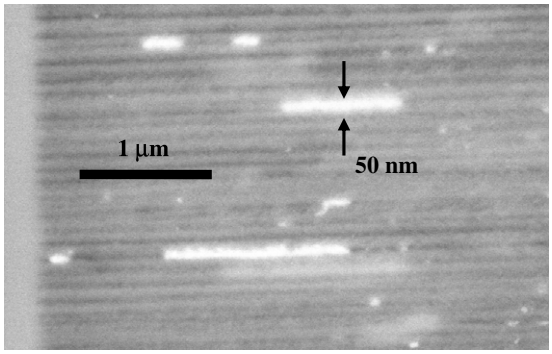

Figure 4. Ni-wires of a few microns in length deposited within the pores of a PS-template.

The metal filling consists of precipitations of various shapes of nanomagnets: spheres, ellipsoids and needles up to a length of a few microns (aspect ratio ∼100) shown in figure 4.

The geometry of the deposited Ni-structures as well as their distribution within the PS-layer can be influenced by the chosen process parameters (current density, pulse duration, electrolyte concentration and temperature) [15]. Chemical characterization with nanoscopic lateral resolution is performed by energy dispersive x-ray spectroscopy to distinguish between the different chemical elements [16]. The precipitated metal nanostructures can more or less homogeneously be deposited over the whole PS-layer, with an accumulation near the surface or at an even higher concentration of Ni near the pore-tips. The influence of the process parameters on the deposition of metal nanostructures gives rise to the opportunity to fabricate samples with desired magnetic properties (e.g. coercivity, remanence, saturation magnetization).

3. Measurements: static magnetization hysteresis

The magnetization properties of oriented Ni-nanowires (figure 4) depend on their orientation with respect to an external magnetic field. Figure 5 displays a strong rise for fields below 1000 G (figure 5(b)). This part is the spin-magnetism of the Ni nanowire system and shows an open loop with coercive forces well below the coherent rotation threshold (which is 3200 G due to shape anisotropy). The dendritic shape of the filled pores provides plenty of nucleation centers for reversed domains along the wire axis reducing the coercive force H_c. Since H_c has the same value for both field directions, strain effects are of minor importance since such effects would induce strong uniaxial magnetoelastic anisotropy and different H_c for each field direction. However in comparison with multidomain bulk Ni ($H_c = 20$ Oe) the anisotropy-field ($\propto H_c$) of wires is enhanced by a factor of at least 10. From the evaluation of the SEM pictures (figures 1–4) we estimate a density of 4×10^8 wires (diameter 50 nm) per mm^2. Taking the saturation magnetization 483 emu cm^{-3} of Ni we estimate, for 1 μm long and 50 nm diameter wires (figure 4) and for a total 3×3 mm^2 sample size, a magnetic moment of 3.4×10^{-3} emu. For a 77% filling factor of Ni in silicon this gives 2.6×10^{-3} emu, not so far from the experimental observation 3×10^{-3} emu (figure 5). Thus the loading of silicon pores is at least 50% and a compact nanomagnetic system can be anticipated.

In figure 5 nearly equal temperature dependencies of the magnetization for both field directions are observed. This fact signals the existence of residual superparamagnetic precipitates of nearly spherical shape. To rule out both this superparamagnetism, as well as the substrate diamagnetism, we simply subtract in figure 6 the magnetizations of both field directions ($M_\parallel - M_\perp$). The result is highly surprising: $M_\parallel - M_\perp$ is nearly linear with magnetic field, does not saturate

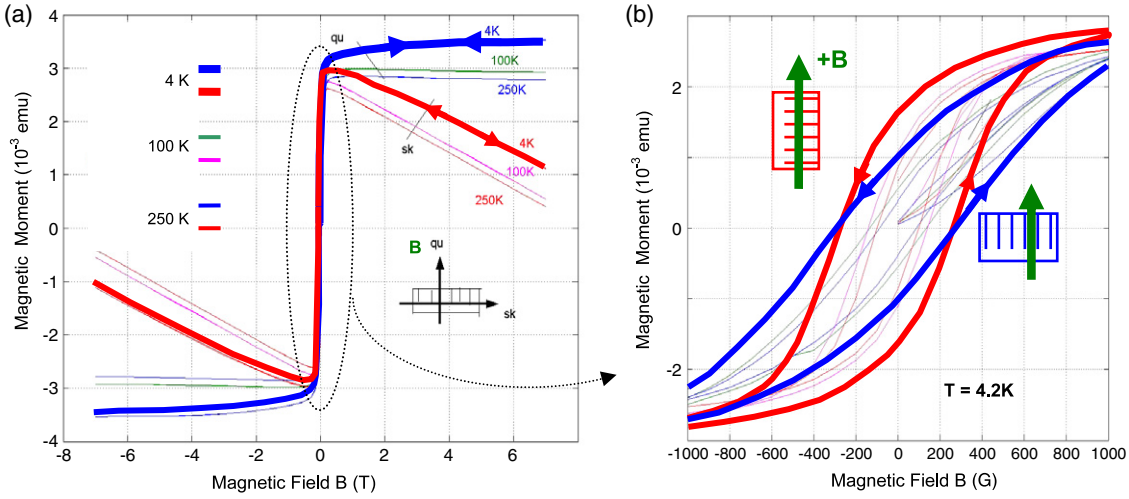

Figure 5. High-field magnetization (a) of a 50 nm-Ni-nanowire array (4×10^8 mm^{-2}) on a 3×3 mm^2 sample. The negative slope for a field perpendicular to the wire axis reflects the diamagnetism of the substrate. Note the nearly perfect compensation of this high amount of diamagnetism by the giant orbital paramagnetism if the field is turned parallel to the wire axis! In the low-field regime (b) the spin-magnetism of Ni is already saturated for fields near 1000 Oe.

(This figure is in colour only in the electronic version)

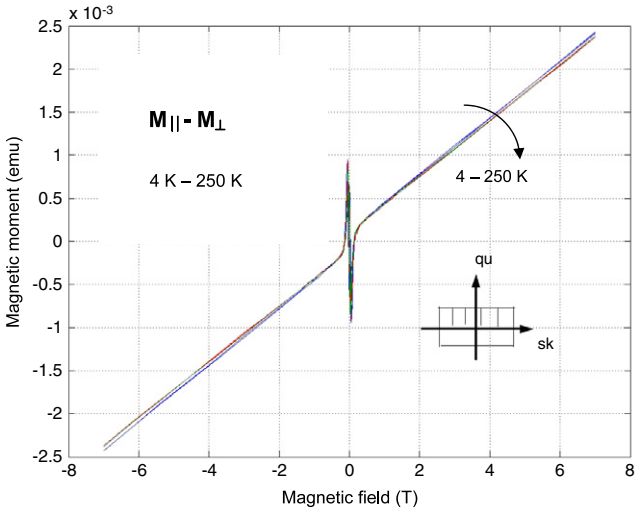

Figure 6. Difference magnetization $M_{\parallel}$–$M_{\perp}$ for fields parallel ($M_{\parallel}$) and perpendicular ($M_{\perp}$) to the wire axis. The wing below 0.1 T occurs from the slight imbalance of the spin-magnetism along with the hysteresis of figure 5(b). Since beyond 0.3 T the spins of Ni are all saturated, the remaining field-linear magnetization is different from spin-related magnetism and reflects the nearly temperature independent giant orbital paramagnetism.

(at least up to 7 T), does not show any hysteresis and is nearly temperature independent.

4. Results and discussion: model of orbital-magnetism and spin-galvanic effect

Orbital-magnetism is based on persistent currents in the mesoscopic regime. It has been observed, e.g. at domain-boundaries of self-assembled organic monolayers on metals [9] or in quantum rings made of a gated two-dimensional electron gas in a semiconductor [17, 18]. The energy of a charged particle of transverse mass m_{T} orbiting around a ring of radius $\langle r\rangle$ in a magnetic field B is quantized in terms of the discrete angular momentum (ℓ) and the magnetic flux quantum $\Phi_0 = h/e$:

$$E_{\ell\uparrow(\downarrow)}(\Phi) = E_{z\uparrow(\downarrow)} + \frac{\hbar^2}{2m_T\langle r\rangle^2}\left(\ell + \frac{\Phi}{\Phi_0}\right)^2 \pm \alpha E_{\mathrm{SO}}\frac{\sqrt{2m_T}}{\hbar}\sqrt{E_{z\uparrow(\downarrow)} + \frac{\hbar^2}{2m_T\langle r\rangle^2}\left(\ell + \frac{\Phi}{\Phi_0}\right)^2}$$
$$\ell = \cdots, -1, 0, 1, 2 \quad \text{magnetic flux } \Phi = \langle r\rangle^2\pi \cdot B. \qquad (1)$$

Since there is a radial symmetry-breaking 'Rashba'-field (E_{SO}) at the hetero-interface between the Ni-wire and silicon, a spin–orbit-interaction $\alpha E_{\mathrm{SO}} \cong 10^{-11}$ eV m [19] induces an increase or decrease ($\pm$) of energy dependent on the spin-direction $\uparrow$ ($\downarrow$). From the Stoner splitting of Ni-spins we expect an imbalance of injected spins in silicon (up to $\approx 10^8$ excess $\uparrow$-spins against $\downarrow$-spins per wire-quadruple, see figure 7). $E_{z\uparrow(\downarrow)}$ is the spin-dependent energy of the free carrier motion along the wire axis. It has been demonstrated in the literature [8], that such a spin-galvanic effect causes a chirality of the orbital motion of the carriers, in our case around the wire-circumference, which can survive even at room temperature.

The magnetic moment M can be figured out from (1) by differentiation of the energy $E_\ell(\Phi)$ with respect to the magnetic field B ($\mu_{\mathrm{B}} = 9.27 \times 10^{-24}$ J T^{-1} is the Bohr magneton):

$$M = -\frac{\partial E_{\ell\uparrow(\downarrow)}(\Phi)}{\partial B} = -\left(1 \pm \frac{\alpha E_{\mathrm{SO}}\sqrt{m_T}/\sqrt{2\hbar^2}}{\sqrt{E_{z\uparrow(\downarrow)} + \frac{\hbar^2}{2m_T\langle r\rangle^2}(\ell + \frac{\Phi}{\Phi_0})^2}}\right)\mu_{\mathrm{B}}\left(\ell + \frac{\Phi}{\Phi_0}\right). \qquad (2)$$

As an estimate, we assume $E_{z\uparrow(\downarrow)} = 0$ and as the lowest possible quantum state $(\ell + \Phi/\Phi_0) = 1$. The sign of the magnetic moment depends on the magnitude of the 'Rashba'-term. For observing paramagnetism the second term in the bracket is, for $\alpha E_{\mathrm{SO}} = 10^{-11}$ eV m [19], $m_{\mathrm{T}} = m_0 = 9 \times 10^{-31}$ kg, $\langle r\rangle = 10.6$ nm (see below) larger than unity, namely $\cong$1.4, thus changing the sign, if the majority spin corresponds to the negative Rashba-term. A sensitive

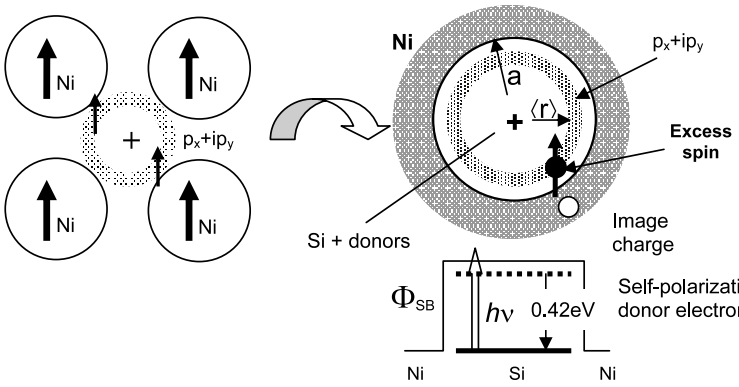

Figure 7. Between 4 Ni-nanowires a Schottky barrier in the depleted silicon bridge is formed. The shallow ionized donor level becomes resonant due to self-polarization by the 'mirror' charge in the metal (simplified cylindrical model on the right part of the figure) and captures spin-polarized carriers from Ni. These carriers occupy the low angular momentum states $\ell = 1, 2, \ldots$ and experience a torque to rotate in one sense of direction due to the spin-galvanic effect [8].

parameter in formula (2) is the radius of the orbit $\langle r \rangle$, which should surmount a minimum value $\langle r \rangle = 8$ nm. To agree with the experiment, a sizable capture of spin-polarized carriers has to be taken into account by impurity-assisted tunneling into silicon from the Ni Fermi level. Due to self-polarization [20] of a captured donor electron induced by the 'mirror' charge in the metal Ni (see the simplified model in the right panel of figure 7) the original shallow level becomes deeper bound ($=-0.42$ eV) within the Schottky barrier Φ_{SB} of the Ni–Si-heterojunction. Such self-polarization is also the responsible self-limiting process for the anodization of porous silicon so that it can be prepared at all [21].

An independent indication of this barrier bound level is the observed infrared absorption at $h\nu = 0.42$ eV [16]. Since Ni is ferromagnetic, imbalanced spins are transferred to this resonant level. The number $\langle N \rangle$ of injected spins can be estimated from equation (2) by multiplying the expression for M with $\langle N \rangle$ per channel, counting the number of channels ($=4 \times 10^9$) and obeying the requirement that the slope of the magnetization curve measured in figure 6 should be reproduced. We estimate $M = 10^{-3}$ emu for $B = 1$ T, $\Phi/\Phi_0 = 0.085$, $\ell = 1$, $\langle N \rangle \cong 2 \times 10^8$ per channel (figure 7), in good agreement with the experiment, using the parameters $2a = 22$ nm (wire separation), $\langle r \rangle = 10.6$ nm (orbital radius of the carriers in silicon), $\varepsilon = 12$ (dielectric constant of silicon). Saturation magnetization of giant paramagnetism is determined by the maximum possible number $\langle N \rangle$ which could be captured in the silicon matrix between a quadruple of Ni-wires.

In summary, the Ni/Si-ferromagnet–semiconductor nanowire system mimics a two-dimensional electron gas in a semiconductor heterostructure exposed to a strong magnetic field. The normally oscillatory susceptibility of such a system is transformed to a giant paramagnetic behavior due to the spin-galvanic effect by which mobile uncompensated spins injected from the ferromagnetic Ni-rods travel around the wires and occupy low angular momentum states. This model explains the experimentally observed strict linear magnetic field dependence, the lack of saturation and the only very weak temperature dependence of the magnetization.

Acknowledgments

This work is dedicated to my (HK) mentor Günther Bauer. It has been financially supported by the Austrian National Science Foundation project No. P18593 and the NAWI-Graz cooperation project. We are indebted for scanning electron microscopy to F Hofer, Institute for Electron Microscopy, Graz University of Technology, and for helpful discussions to F Kuchar, R Meisel and C Brunner, University of Leoben, Austria.

References

[1] Lee W, Schwirn K, Steinhart M, Pippel E, Scholz R and Gösele U 2008 *Nat. Nanotechnol.* **3** 234
[2] Nielsch K, Wehrspon R B, Barthel J, Kirschner J and Gösele U 2001 *Appl. Phys. Lett.* **79** 1360
[3] Whitney T M, Jiang J S, Searson P C and Chien C L 1993 *Science* **261** 1316
[4] Sellmyer D J, Zheng M and Skomski R 2001 *J. Phys.: Condens. Matter* **13** R433
[5] Frei E H, Shtrikman S and Treves D 1957 *Phys. Rev.* **106** 446
[6] Sinova J, Culcer D, Niu Q, Sinitsyn N A, Jungwirth T and MacDonald A H 2004 *Phys. Rev. Lett.* **92** 126603
[7] Bernevig B A, Hughes T L and Zhang S C 2005 *Phys. Rev. Lett.* **95** 066601
[8] Ganichev S D, Ivchenko E L, Bel'kov V V, Tarasenko S A, Sollinger M, Weiss D, Wegscheider W and Prettl W 2002 *Nature* **417** 153
[9] Hernando A, Crespo P and Garcia M A 2006 *Phys. Rev. Lett.* **96** 057206
[10] Kuemmeth F, Ilani S, Ralph D C and McEuen P L 2008 *Nature* **452** 448
[11] Vager Z and Naaman R 2004 *Phys. Rev. Lett.* **92** 087205
[12] Föll H, Christophersen M, Carstensen J and Hasse G 2002 *Mater. Eng.* R **39** 93
[13] Canham L T, Cullis A G, Pickering C, Dosser O D, Cox T I and Lynch T P 1994 *Nature* **368** 133
[14] Rönnebeck S, Carstensen J, Ottow S and Föll H 1999 *Electrochem. Solid State Lett.* **2** 126
[15] Granitzer P, Rumpf K, Pölt P, Reichmann A and Krenn H 2007 *Physica* E **38** 205
[16] Rumpf K, Granitzer P, Pölt P, Reichmann A and Krenn H 2006 *Thin Solid Films* **515** 716
[17] Chakraborty T and Pietiläinen P 1994 *Phys. Rev.* B **50** 8460
[18] Fuhrer A, Lüscher S, Ihn T, Heinzel T, Ensslin K, Wegscheider W and Bichler M 2001 *Nature* **413** 822
[19] Inoue J, Bauer G E W and Molenkamp L W 2003 *Phys. Rev.* B **67** 033104
[20] Babic D, Tsu R and Greene F 1992 *Phys. Rev.* B **45** 14150
[21] Tsu R and Babic D 1995 *Porous Silicon Science and Technology* ed J-C Vial and J Derrien (Berlin: Springer) p 111